



# Intra-urban Variations of the CO<sub>2</sub> Fluxes at the Surface-Atmosphere Interface in the Seoul Metropolitan Area

Seon-Ok Hong<sup>1,2</sup> · Jinwon Kim<sup>3</sup> · Young-Hwa Byun<sup>3</sup> · Jinkyu Hong<sup>4</sup> · Je-Woo Hong<sup>5</sup> · Keunmin Lee<sup>4</sup> · Young-San Park<sup>1</sup> · Sang-Sam Lee<sup>1</sup> · Yeon-Hee Kim<sup>6</sup>

Received: 27 October 2022 / Revised: 17 March 2023 / Accepted: 25 March 2023 / Published online: 12 April 2023  
© The Author(s) 2023

## Abstract

Severe spatiotemporal heterogeneity of emissions sources and limited measurement networks have been hampering the monitoring and understanding of CO<sub>2</sub> fluxes in large cities, a great concern in climate research as big cities are among the major sources of anthropogenic CO<sub>2</sub> in the climate system. To understand the CO<sub>2</sub> fluxes in Seoul, Korea, CO<sub>2</sub> fluxes at eight surface energy balance sites, six urban (vegetation-area fraction < 15%) and two suburban (vegetation-area fraction > 60%), for 2017–2018 are analyzed and attributed to the local land-use and business types. The analyses show that the CO<sub>2</sub> flux variations at the suburban sites are mainly driven by vegetation and that the CO<sub>2</sub> flux differences between the urban and suburban sites originate from the differences in the vegetation-area fraction and anthropogenic CO<sub>2</sub> emissions. For the CO<sub>2</sub> fluxes at the urban sites; (1) vehicle traffic (traffic) and heating-fuel consumption (heating) contribute > 80% to the total, (2) vegetation effects are minimal, (3) the seasonal cycle is driven mainly by heating, (4) the contribution of heating is positively related to the building-area fraction, (5) the annual total is positively (negatively) correlated with the commercial-area (residential-area) fraction, and (6) the traffic at the commercial sites depend further on the main business types to induce distinct CO<sub>2</sub> flux weekly cycles. This study shows that understanding and estimation of CO<sub>2</sub> fluxes in large urban areas require careful site selections and analyses based on detailed consideration of the land-use and business types refined beyond the single representative land-use type widely-used in contemporary studies.

**Keywords** Urban CO<sub>2</sub> fluxes · Eddy correlation method · Landuse-business types · Heating-fuel consumption · Vehicle traffic · Carbon cycle

Responsible Editor: Yun Gon Lee.

✉ Jinwon Kim  
jkim@atmos.ucla.edu

Seon-Ok Hong  
seonok0421@korea.kr

Young-Hwa Byun  
yhbyun@korea.kr

Jinkyu Hong  
jhong@yonsei.ac.kr

Je-Woo Hong  
jwhong@kei.re.kr

Keunmin Lee  
km.lee@yonsei.ac.kr

Young-San Park  
sanpark@korea.kr

Sang-Sam Lee  
sangsam.lee@korea.kr

Yeon-Hee Kim  
kyh@kma.go.kr

- 1 Research Applications Department, NIMS, Seogwipo-Si, Jeju-Do, Republic of Korea
- 2 Present Address: Observation Research Department, NIMS/KMA, Seogwipo-si, Jeju-do, Republic of Korea
- 3 Climate Change Research Team, NIMS, Seogwipo-Si, Jeju-Do, Republic of Korea
- 4 Department of Atmospheric Sciences, Yonsei University, Seoul, Republic of Korea
- 5 Korea Adaptation Center for Climate Change, KEI, Sejong, Republic of Korea
- 6 Numerical Modeling Center, KMA, Daejeon, Republic of Korea

## 1 Introduction

Monitoring of carbon dioxide (CO<sub>2</sub>) emissions in urban areas is a critical concern in climate research because cities are among the key contributors to the global climate change induced by the emissions of anthropogenic greenhouse gases (GHGs). Generation of the energy to support the massive populations, industries, human activities, and infrastructure in large cities relies heavily on fossil fuel combustions to emit massive amounts of CO<sub>2</sub> into the climate system. Currently, the fossil- and biofuel combustions in urban areas contribute about 70% of the global CO<sub>2</sub> emissions (Canadell and Raupach 2009; Satterthwaite et al. 2008). As urban populations are expected to grow in the future, from 55% of the world population in 2018 to 68% in 2050 (UN 2019), the contribution of urban areas to the global CO<sub>2</sub> emissions will continue to increase. Thus, monitoring and understanding of urban CO<sub>2</sub> fluxes are important not only for projecting future climate change (Kennedy et al. 2010; Soegaard and Møller-Jensen 2003) but also for evaluating indirect CO<sub>2</sub> emissions estimates based on various methods, for example, inverse modeling, inventory (or bottom-up) method, and satellite-based analyses, that are widely used for tracking how well each nation or region conforms to the emissions limits mandated by international treaties like the Paris Agreement (UNFCCC 2015).

CO<sub>2</sub> fluxes in an urban area vary following the regional climate, seasons, land-use types, and businesses types, as these factors affect key sources and sinks of CO<sub>2</sub>. Human activities such as transportation, heating, power generation, manufacturing, maritime ports and airports as well as metabolic respiration are the main CO<sub>2</sub> sources while vegetation in parks, urban forests, and croplands are the major CO<sub>2</sub> sinks during the growing season (Christen 2014; Coutts et al. 2007; Crawford and Christen 2015; Grimmond and Christen 2012; Helfter et al. 2011, 2016; Hong et al. 2020; Kennedy et al. 2009; Kurppa et al. 2015; Lee et al. 2021; Stagakis et al. 2019; Velasco and Roth 2010; Vogt et al. 2006; Ward et al. 2015; Weissert et al. 2014). Velasco and Roth (2010) compared CO<sub>2</sub> emissions for over 30 midlatitude urban sites to show that most of the CO<sub>2</sub> emissions variations among cities are attributable to the vehicle traffic (traffic, hereafter) and heating-fuel consumption (heating, hereafter). Seasonal variations in heating and CO<sub>2</sub> uptakes by vegetation also result in distinct seasonal variations in urban CO<sub>2</sub> fluxes, especially in the midlatitudes where the seasonal temperature contrast is large (Lee et al. 2021; Moriwaki and Kanda 2004; Ward et al. 2015). Differences in the land-use and business types also draw different traffic and heating patterns to result in large CO<sub>2</sub> flux variations over a heterogeneous landscape

(Gokhale 2011; Hong et al. 2020; Lee et al. 2014a). For example, previous studies (e.g., Nemitz et al. 2002; Soegaard and Møller-Jensen 2003; Velasco et al. 2005) found that the traffic and floating population patterns vary following the main business types (e.g., company headquarters, government offices, retail shops, entertainments) to result in heterogeneous CO<sub>2</sub> flux diurnal cycles.

Large spatial and temporal variations in CO<sub>2</sub> fluxes following the land-use and business types pose a great challenge in monitoring and quantifying CO<sub>2</sub> fluxes over large urban areas. Various methodologies have been attempted to obtain CO<sub>2</sub> fluxes over and/or within various source areas. Inventory methods that calculate the monthly or annual CO<sub>2</sub> fluxes from various sources within a region of interests using the records of energy use, especially the combustion of fossil fuels (Kennedy et al. 2010) have been widely used, but suffer from the lack of temporal and spatial resolutions for identifying local CO<sub>2</sub> emissions sources and their intensities as well as the inaccurate emissions reporting by local emitters (Asefi-Najafabady et al. 2014; Sargent et al. 2018). In addition, the inventory method is only applicable to monitor the emissions from anthropogenic sources. Inverse modeling methods (e.g., Manning et al. 2011; Henne et al. 2016) have also been used to estimate the net emissions of trace gases from both natural and anthropogenic sources and sinks at various spatiotemporal scales within a region of interests on the basis of the observed trace-gas concentrations and atmospheric data in conjunction with an inverse model. Peters et al. (2007) used an inverse model, the CarbonTracker, to estimate the surface CO<sub>2</sub> fluxes over the North America. Lauvaux et al. (2016) established a fine-scale CO<sub>2</sub> emissions monitoring system for the City of Indianapolis, United States of America, using an inverse modeling method. Despite successful applications of inverse modeling to the estimation of regional emissions of CO<sub>2</sub> and other trace gases, the method is susceptible to model errors as well as the uncertainty in input data related to their accuracies and the spatiotemporal coverages, especially for urban areas which require fine-scale input data (Lauvaux et al. 2016) due to rapidly varying, both temporally and spatially, meteorology and emissions sources. Satellite data also have been used to estimate CO<sub>2</sub> emissions from large urban areas (e.g., Labzovskii et al. 2019; Shim et al. 2019), but they lack the spatial resolutions for identifying intra-urban variations. In addition, all indirect CO<sub>2</sub> flux estimates need to be verified against directly measured in-situ data. Thus, direct measurements of surface CO<sub>2</sub> fluxes at multiple urban sites are sorely needed not only for understanding urban CO<sub>2</sub> fluxes but also for evaluating CO<sub>2</sub> flux estimates based on indirect methods.

The eddy covariance (EC) method that calculates trace-gas fluxes as the covariance of trace-gas concentrations and

atmospheric variables obtained using high-frequency sensors has been the fundamental tool for direct measurements of the energy and CO<sub>2</sub> exchanges at the surface-atmosphere interface (Baldochi et al. 2001; Moriwaki and Kanda 2004; Soegaard and Møller-Jensen 2003; Velasco et al. 2005). The EC method allows continuous monitoring of surface CO<sub>2</sub> fluxes at fine temporal resolutions, typically from 30 min to 1 h. Because fluxes observed at the same site vary following wind directions and speeds if the sources and sinks of the trace-gas around the site are spatially and/or temporally heterogeneous, the high-rate sampling capability of the EC method is advantageous for monitoring CO<sub>2</sub> fluxes and understanding the carbon cycle related to urban ecosystems (Feigenwinter et al. 2012). A number of studies successfully quantified CO<sub>2</sub> fluxes and their variabilities, as well as the key elements that affect CO<sub>2</sub> fluxes at various urban areas, using the EC method (e.g., Coutts et al. 2007; Lietzke et al. 2015; Velasco and Roth 2010; Ward et al. 2015; Hong et al. 2019, 2020; Park et al. 2022). Previous urban CO<sub>2</sub> flux studies typically analyzed the differences between cities, or, for the same city, between different periods using data from a single site (e.g., Coutts et al. 2007; Velasco and Roth 2010). Because CO<sub>2</sub> fluxes vary widely according to the land-use and main business types, the CO<sub>2</sub> flux characteristics in large urban areas that include diverse landscapes and human activities cannot be represented by single-site measurements (Grimmond et al. 2002; Kleingeld et al. 2018; Park et al. 2022).

In order to understand the variations of CO<sub>2</sub> fluxes in a large urban area, this study analyzes the CO<sub>2</sub> flux data obtained using the EC method at eight surface energy balance (SEB) sites of the Korea Meteorological Administration (KMA) within the Seoul metropolitan area (Seoul, hereafter) (Choi et al. 2013; Park et al. 2017) over the two-year period from January 2017 to December 2018. Seoul shows one of the largest CO<sub>2</sub> concentration anomalies in the world with large seasonal variations. A number of studies have investigated the CO<sub>2</sub> budget for Seoul on the basis of CO<sub>2</sub> concentration data from various sources such as satellites (Labzovskii et al. 2019; Shim et al. 2019; Park et al. 2020) and ground-based measurements (Park et al. 2021). These past studies provide useful insights into the CO<sub>2</sub> budget over Seoul, but lack the spatial resolution for understanding the intra-urban scale variations of CO<sub>2</sub> fluxes within Seoul. Recently, Park et al. (2022) analyzed EC data measured at multiple sites in Seoul to show that CO<sub>2</sub> fluxes are strongly affected by local sources and sinks that can be described by local land-use types.

This study analyzes the CO<sub>2</sub> fluxes measured at eight EC sites in the Seoul metropolitan area and attempts to relate the fluxes to a variety of local factors such as the types of land-use and main businesses within the flux footprint of each site. Unlike past studies which assign a single dominant land-use type to each site (e.g., Hong et al. 2019; Park et al.

2022), this study considers in addition to the contemporary site type assignment, more refined local land-use factors such as the area fraction of multiple land-use types and, for the commercial area, the main business type, to understand the variations of the observed fluxes. This paper is organized as follows. The EC sites and data processing methods employed in this study are presented in Sect. 2. Section 3 presents the analyzed CO<sub>2</sub> flux variations and their relationship to local factors including the types of land-use and main businesses (or commerce) as well as human activities related to the characteristics of each site. Conclusions and discussions are presented in Sect. 4.

## 2 Data and Methods

### 2.1 Observation Sites

This study analyzes the CO<sub>2</sub> flux data measured at eight SEB sites (Fig. 1) in the KMA Urban Meteorological Observation System (Park et al. 2017) for the two-year period from January 2017 to December 2018. Table 1 presents the specific information on these sites such as the geographical location, local climate zone (LCZ), sensor installation, and the parameters related to land-use types. All of the eight SEB sites are located on flat terrain with minimal terrain slopes. Seven of the eight SEB sites are located at building roof tops of various heights, from 4 to 71 m above the ground level (AGL); the remaining one site (BC) is located at the ground level with EC sensors installed at 10 m AGL. The roughness length ( $z_0$ ) and displacement height ( $z_d$ ) are computed following Kanda et al. (2013) using the building data within 250 m of each site from the Digital Map 2.0 Building (An et al. 2020). For all sites, the true sensor height defined as the sum of the building height (BH) and sensor height (SH), exceeds twice of the mean BH (MBH) within 250 m. Thus, the SEB sensors at all of the eight sites are located in the inertial sublayer, also known as the constant flux layer, that typically exists above twice of the MBH (Barlow 2014; Raupach et al. 1991).

AY, an LCZ 4E site with a large commercial-area fraction, is mainly composed of retail shops, restaurants, and pubs that attract a large floating population and traffic in both daytimes and evenings. GHM, also of LCZ 4E with a large commercial-area fraction, includes mainly government offices, company headquarters, and the businesses related to them which are open mostly during the work hours on weekdays. NW, an LCZ 5E site, includes a railway depot and a driver's license driving test facility in 500 m to the north and a residential building complex to the south. The driving test facility next to the NW site operates only during the weekday work hours. Note that the driving test vehicles are not included in the local traffic count as the facility is

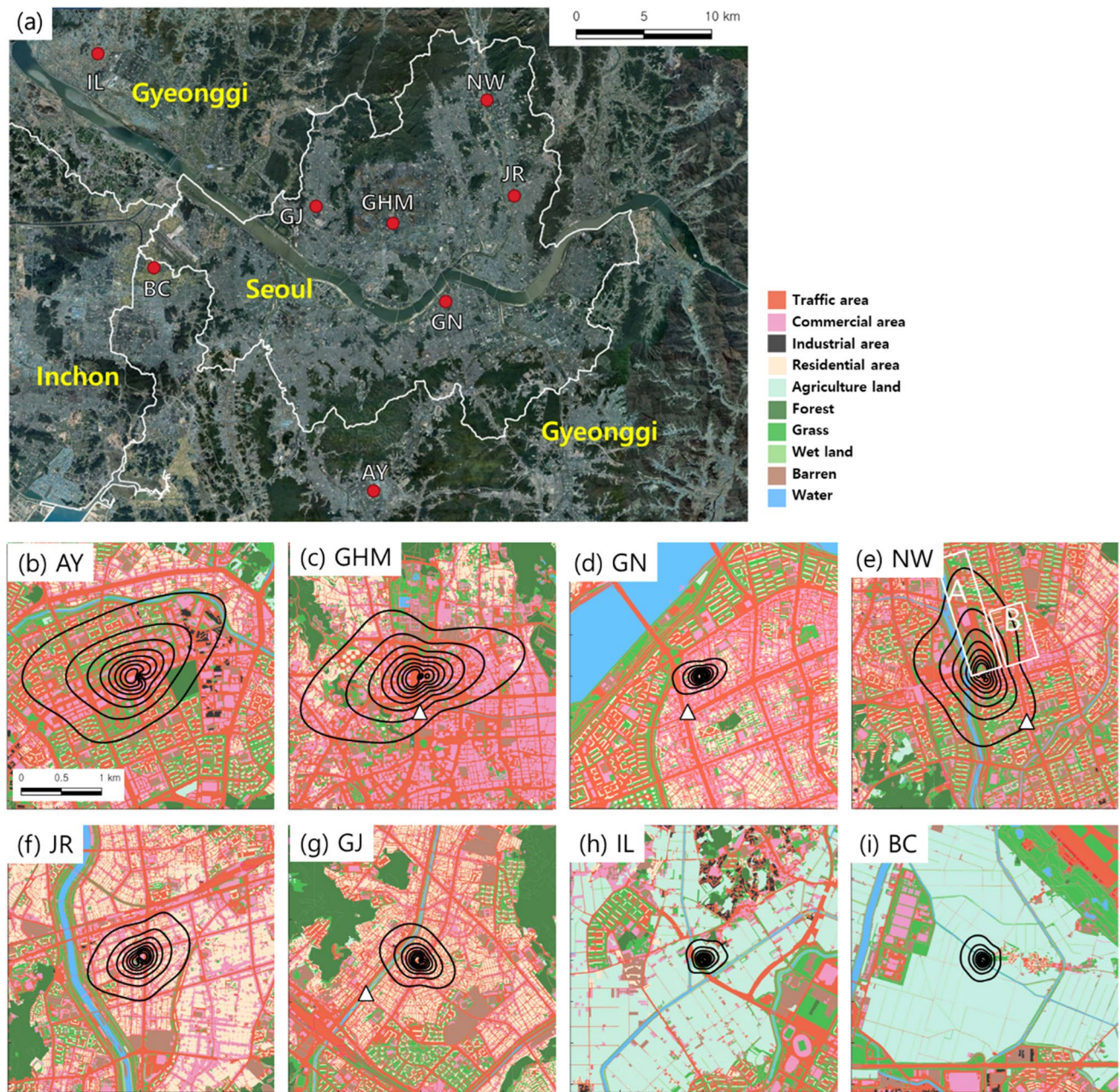


**Fig. 1** (a) A satellite image of the Seoul metropolitan area and the locations of the eight SEB sites (red dots) used in this study. Also shown are the satellite images of the individual SEB sites in Table 1: (b) AY (Anyang), (c) GHM (Gwanghwamun), (d) GN (Gangnam), (e) NW (Nowon), (f) JR (Jungnang), (g) GJ (Gajwa), (h) IL (Ilsan), and (i) BC (Bucheon). The white squares A and B in (e) indicate the

railway depot and the driver's license driving test facility, respectively. The white triangles in (c), (d), (e), and (g) indicate the locations of traffic monitoring cameras that provide the traffic volume analyzed in this study. The black contour lines specify the flux footprint climatology from 10 to 80% over two-years (2017–2018)

not covered by any traffic monitoring cameras. GN, an LCZ 2E site, includes mid-rise residential and commercial buildings in its immediate vicinity with high-rise commercial and residential buildings to the southwest and northwest, respectively. Despite the residential-area fraction around GN is large (40.8%), the site is strongly affected by heavy concentrations of retail shops in strip malls and shopping districts,

restaurants, pubs, entertainment businesses, and traffic hubs, that draw large traffic and floating populations during work hours as well as evenings in both weekdays and weekends. JR (LCZ 3E) and GJ (LCZ 2E) is composed mainly of low-rise and compact mid-rise residential buildings, respectively, and the retail shops that serve mainly local residents. The two suburban sites BC and IL belong to LCZ 9D. BC

**Table 1** Site characteristics and surface type of the study sites

Category	Site	<sup>1)</sup> LCZ	Lat/ Long	Alt. (m)	<sup>2)</sup> BH (m)	<sup>3)</sup> SH (m)	z <sub>0</sub> (m)	z <sub>d</sub> (m)	<sup>4)</sup> MBH (m)	<sup>5)</sup> λ <sub>p</sub>
Urban sites	Anyang (AY)	4E	37.394N/ 126.962E	37.0	64.0	6.0	5.6	37.4	30.7	0.3
	Gwang-hwamun (GHM)	4E	37.572N/ 126.978E	43.0	71.0	7.0	4.9	37.5	33.0	0.3
	Nowon (NW)	5E	37.654N/ 127.057E	38.0	37.5	10.0	2.3	15.3	15.0	0.2
	Gangnam (GN)	2E	37.520N/ 127.022E	26.0	21.2	4.0	1.4	17.2	13.0	0.4
	Jungnang (JR)	3E	37.591N/ 127.079E	22.0	23.0	18.5	1.0	12.3	9.4	0.4
	Gajwa (GJ)	2E	37.58N/ 126.91E	21.0	23.0	6.0	1.4	15.1	11.5	0.4
Suburban sites	Ilsan (IL)	9D	37.685N/ 126.731E	9.0	4.0	10.0	-	-	-	-
	Bucheon (BC)	9D	37.543N/ 126.778E	10.0	0.0	10.0	0.1	1.7	3.1	0.1

<sup>1)</sup> Stewart and Oke (2012) local climate zones (LCZ): Classified using MBH and λ<sub>p</sub>. 2, compact mid-rise; 4, open high-rise; 5, Open mid-rise, 9, sparsely built; D, low plant; E, bare rock or paved

<sup>2)</sup>BH: Building Height (above ground level)

<sup>3)</sup>SH: Sensor Height above rooftop or ground

<sup>4)</sup>MBH: Mean Building Height in 250 m radius of station

<sup>5)</sup>λ<sub>p</sub>: The building plan area fraction in 250 m radius of station

includes mostly agricultural lands with minimal building-area fraction (1.2%) and traffic-area fraction (1.9%). IL also includes mainly agricultural lands with small building-area fraction (6.9%); however, unlike BC, it includes a major road (traffic-area fraction of 28.4%) to the southwest.

## 2.2 Data and Quality Control

The SEB sites monitor at 10 Hz sampling rates the three wind components (*u*, *v*, *w*) and sonic temperatures (*T<sub>s</sub>*) using a 3-dimensional sonic anemometer (CSAT3, Campbell Scientific, USA) as well as the trace-gas (CO<sub>2</sub>, H<sub>2</sub>O) concentrations, ambient temperatures, and ambient pressures using open-path infrared CO<sub>2</sub>/H<sub>2</sub>O gas analyzers (EC150, Campbell Scientific, USA). A collocated automated weather station (AWS) measures conventional meteorological data such as pressure, winds, temperatures, relative humidity, short- and longwave radiation, the net radiation and precipitation, at 1-min intervals. The observed data are archived using a data logger (CR3000, Campbell Scientific, USA). Sensor details for each SEB site are referred to Park et al. (2017).

Quality control (QC) of the high-frequency data (*u*, *v*, *w*, *T<sub>s</sub>*, CO<sub>2</sub>, H<sub>2</sub>O) employs the double-rotation and spike-removal method of Vickers and Mahrt (1997). The CO<sub>2</sub> fluxes are computed based on the EC method by determining the covariance of the vertical wind velocity (*w*) and

CO<sub>2</sub> concentration measured by the high-frequency sensors using the EddyPro software version 7.0.6 (Li-COR, USA) at 30-min intervals. The EddyPro software is also used to QC the flux data by incorporating key options such as; the spectral corrections with the analytic options of the low-pass filtering and high-pass filtering effects (Moncrieff et al. 1997, 2004), the Webb-Pearman-Leuning (WPL) method for the air volume and density fluctuation corrections (Webb et al. 1980), and the Foken and Wichura (1996) steady-state and integral turbulence characteristic (ITC) tests. The Foken and Wichura test (Foken and Wichura 1996) assigns quality flags (QF) to each 30-min flux value based on the steady-state and ITC tests such that: QF 1–3 can be used in fundamental research such as the development of parameterizations while QF 4–6 are applicable to general uses including constructions of CO<sub>2</sub> budgets at longer timescales. The analyses in this study utilizes the flux data of QF 1–6. Missing data filling, an essential step in calculating the CO<sub>2</sub> flux budget over various extended time scales (Dragomir et al. 2012; Falge et al. 2001), is performed using the mean diurnal variation (MDV) method of Falge et al. (2001) which fills a missing data using the mean diurnal cycle of the fluxes within the 14-day window centered on the day of missing data. After applying the QC and gap filling, the resulting 30-min flux data covers 72.1%–91.0% of the entire analysis period for all sites.

### 2.3 Source-Area Modelling and Land-Use Weighting

Two-year (2017–18) ensemble flux source-area footprint of each SEB site is constructed at 10 m resolutions over a  $400 \times 400$  (4 km  $\times$  4 km) grid nest using the Flux Footprint Prediction (FFP) model of Kljun et al. (2015). The input data for the FFP model include the aerodynamic variables such as the standard deviation of the lateral velocity with respect to the double-rotation axis (see the data QC section), wind direction, friction velocity ( $u_*$ ), the Monin–Obukhov length ( $L$ ), the planetary boundary layer height (PBLH), and the geomorphological variables including the roughness length ( $z_0$ ) and displacement height ( $z_d$ ). The geomorphological data of each site are described in Sect. 2.1 and Table 1. The aerodynamic input data are obtained from the EC data in 30-min intervals. The resulting ensemble flux footprint climatology at each SEB site (Fig. 1) shows that the footprint-area size depends strongly on the sensor heights as the smallest footprint areas occur at the sites of the lowest sensor heights (GN, GJ, IL, and BC).

The weighted land-use fraction for classifying the land-use types of each site is calculated using the Stagakis et al. (2019) method in conjunction with the ensemble source-area footprint data and the 3 m-resolution land-use type data of the Environmental Geographic Information Service (EGIS), the Ministry of Environment, Korea (available at <https://egis.me.go.kr>). The Stagakis et al. (2019) method calculates the weighted land-use fraction ( $w_i$ ) of each land-use type ( $i$ ), the relative contribution of the land-use type  $i$  within the ensemble flux source-area footprint to the measured  $\text{CO}_2$  flux, by first multiplying the flux source-area footprint value ( $\varphi(x, y)$ ) by the land-use type fraction ( $\lambda_i(x, y)$ ) at the 10 m-resolution

grid box ( $x, y$ ), then summing the grid-point values over the entire area of interests:

$$w_i = \sum_{x=1}^{400} \sum_{y=1}^{400} \varphi(x, y) \lambda_i(x, y) \quad (1)$$

The weighted land-use fraction in (1) is called ‘land-use type fraction’ hereafter.

$\text{CO}_2$  fluxes vary according to the land-use and business types as they shape the local traffic, floating population, heating (the primary  $\text{CO}_2$  sources), and other energy consumption types, as well as the amount of vegetation (the primary  $\text{CO}_2$  sinks). In order to understand the  $\text{CO}_2$  flux variations in Seoul, the eight SEB sites are grouped into six urban and two suburban sites (Table 1) on the basis of the vegetation-area fraction (Fig. 2; Table 2). The two suburban sites are characterized by large vegetation-area fractions (61.9% at IL and 94.4% at BC) while the vegetation-area fractions at the six urban sites are small, from 1.6% at GN to 14.7% at NW. The traffic-, commercial-, and residential-area fraction at the six urban sites vary in the ranges 28.7–62.4%, 17.1–30.8%, and 2.4–40.8%, respectively (Table 2). The combined fraction of the commercial, residential, paved non-road, and paved road areas is 79% or more for the six urban sites.

## 3 Results

### 3.1 Annual and Seasonal $\text{CO}_2$ Fluxes

The annual  $\text{CO}_2$  fluxes at the eight SEB sites range from  $0.026 \text{ mg CO}_2 \text{ m}^{-2} \text{ s}^{-1}$  ( $0.83 \text{ kgCO}_2 \text{ m}^{-2} \text{ yr}^{-1}$ ) at BC to  $1.14$

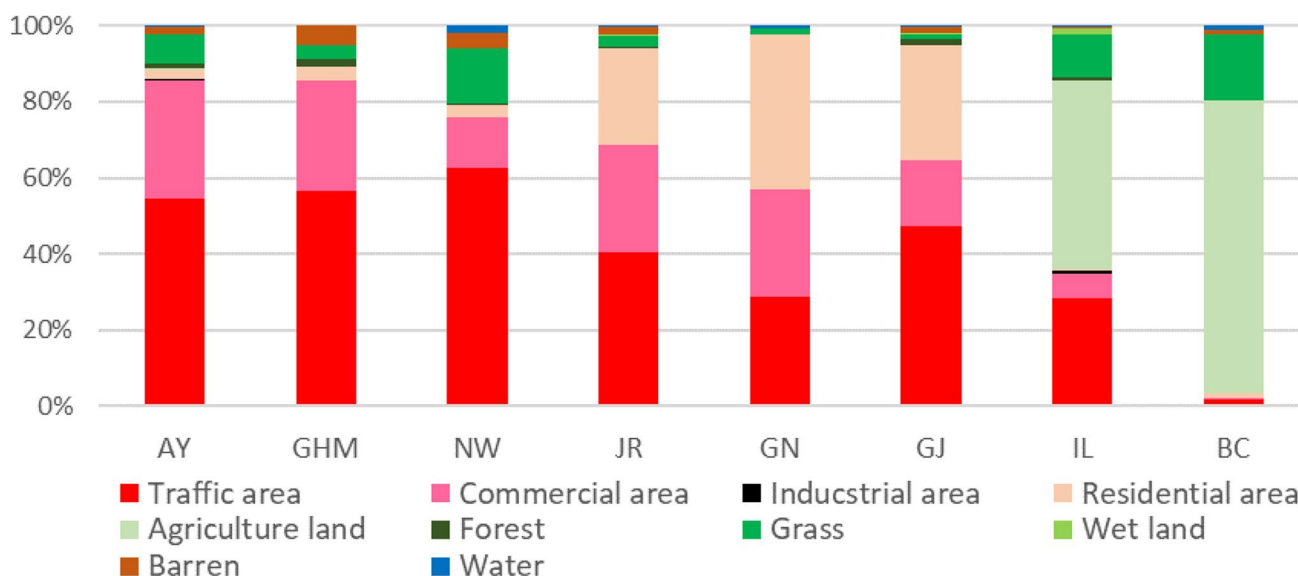


Fig. 2 The land-use fraction at each site based on the 2-year climatological footprint

**Table 2** The values of the fractional areas of key urban components (urban area, vegetation area, traffic area, commercial area, and residential area)

	Site	*Urban Area (%)	Vegetation Area (%)	Traffic Area (%)	Commercial Area (%)	Residential Area (%)	Building (Residential + Commercial) Area (%)
Urban site	AY	87.8	9.1	54.6	30.8	2.4	33.2
	GHM	89.3	5.4	56.6	28.8	3.9	32.7
	**NW	79.2	14.7	62.4	13.6	3.2	16.8
	JR	94.1	3.4	40.5	28.1	25.5	53.6
	GN	97.6	1.6	28.7	28.1	40.8	68.9
	GJ	94.7	2.6	47.3	17.1	30.3	47.4
Suburban site	IL	35.3	61.9	28.4	6.6	0.3	6.9
	BC	3.1	94.4	1.9	0.3	0.9	1.2

\*The urban-area fraction is the sum of the fractions of traffic area, commercial area, and residential area

\*\* A large portion of the traffic area at NW are the driver's license driving test facility and a railway depot. The traffic in these areas are not monitored by traffic camera

mgCO<sub>2</sub> m<sup>-2</sup> s<sup>-1</sup> (35.8 kgCO<sub>2</sub> m<sup>-2</sup> yr<sup>-1</sup>) at AY (Fig. 3a). These numbers are well within the range reported for various urban areas around the world (e.g., 10.8 kgCO<sub>2</sub> m<sup>-2</sup> yr<sup>-1</sup> for Łódź, Poland (Pawlak et al. 2011); 36.7 kgCO<sub>2</sub> m<sup>-2</sup> yr<sup>-1</sup> for Edinburgh, UK (Nemitz et al. 2002); 1.3 kgCO<sub>2</sub> m<sup>-2</sup> yr<sup>-1</sup> for a heavily vegetated suburban area in Maryland, US (Crawford and Christen 2015); 10.1 kgCO<sub>2</sub> m<sup>-2</sup> yr<sup>-1</sup> for Seoul, Korea (Hong et al. 2019); 1.09–16.28 kgC (4.0–59.75 kgCO<sub>2</sub>) m<sup>-2</sup> yr<sup>-1</sup> for Seoul (Park et al. 2022)). The large variations within Seoul (Park et al. 2022) show that CO<sub>2</sub> fluxes vary widely due to highly heterogeneous land-use types and business types as explored in later sections. The seasonal-mean CO<sub>2</sub> fluxes are much larger in winter (red) than in summer (Fig. 3a), suggesting that heating is among the main CO<sub>2</sub> emissions sources in winter for all urban sites where the vegetation-area fractions are minimal (Park et al. 2014, 2022). The two suburban sites characterized by large vegetation-area fractions and minimal anthropogenic CO<sub>2</sub> sources, yield the smallest annual and seasonal CO<sub>2</sub> fluxes. The small CO<sub>2</sub> fluxes at the suburban sites in summer, near-zero at IL and negative at BC (Fig. 3a), indicate that vegetation plays a critical role in the CO<sub>2</sub> budget at the vegetation-rich suburban sites in summer (Ward et al. 2015). Despite the large CO<sub>2</sub> removal by vegetation during summer, the seasonal contrasts (i.e., the difference between summer and winter) in the CO<sub>2</sub> fluxes at the two suburban sites (0.19 and 0.37 mgCO<sub>2</sub> m<sup>-2</sup> s<sup>-1</sup> at IL and BC, respectively) are much smaller than those at the urban sites (0.46–0.96 mgCO<sub>2</sub> m<sup>-2</sup> s<sup>-1</sup>), especially at BC.

Strong contrasts exist in the annual and seasonal CO<sub>2</sub> fluxes between the urban and suburban sites (Fig. 3b-d). The annual flux averaged over the urban- and suburban sites is 0.89 and 0.14 mgCO<sub>2</sub> m<sup>-2</sup> s<sup>-1</sup> respectively, i.e., on average, the urban sites emit six times larger CO<sub>2</sub> per unit area than the suburban sites. Seasonally, the differences between the

urban- and suburban sites (Fig. 3c,d) are related well to the differences in the vegetation-area fraction like the annual value. For the mean flux over the entire corresponding sites, the difference between the urban- and suburban group is much larger in winter (1.34 vs. 0.27 mgCO<sub>2</sub> m<sup>-2</sup> s<sup>-1</sup>) than in summer (0.67 vs. -0.01 mgCO<sub>2</sub> m<sup>-2</sup> s<sup>-1</sup>). This indicates that the difference in the observed CO<sub>2</sub> fluxes between the urban and suburban sites comes from the differences primarily in the anthropogenic CO<sub>2</sub> emissions and secondarily in the CO<sub>2</sub> removal by vegetation. Note that a larger vegetation-area fraction implies a smaller fraction of urban-type (combined the commercial, residential, and traffic area) area that emits much larger CO<sub>2</sub> than the vegetation area (Park et al. 2022). Thus, the CO<sub>2</sub> flux differences between summer and winter come primarily from different seasonal CO<sub>2</sub> uptakes by vegetation (the seasonal anthropogenic CO<sub>2</sub> emissions) for the two suburban (six urban) sites. It must be noted that the CO<sub>2</sub> fluxes at the six urban sites are poorly related to the vegetation-area fraction for the entire year as well as for both seasons (Fig. 3b-d). Considering that even the largest correlation coefficient between the CO<sub>2</sub> fluxes and the vegetation-area flux at the urban sites for summer (0.43) is below the 60% statistical significance level, the CO<sub>2</sub> fluxes at the urban sites are almost entirely determined by the anthropogenic CO<sub>2</sub> emissions with negligible contributions from vegetation. This result contrasts one of the key findings in Park et al. (2022) who argue that the role of vegetation is critical in the CO<sub>2</sub> budget at all urban sites.

The large downward fluxes in the sunlit hours of summer (Fig. 4) at the two suburban sites clearly demonstrate the critical role of vegetation in shaping the seasonal CO<sub>2</sub> flux budget in the regions of large vegetation cover (Ward et al. 2015; Velasco and Roth 2010; Velasco et al. 2013). The daytime minima in the annual-mean and summer CO<sub>2</sub> flux diurnal cycle appear clearly in summer (red lines in Fig. 4)

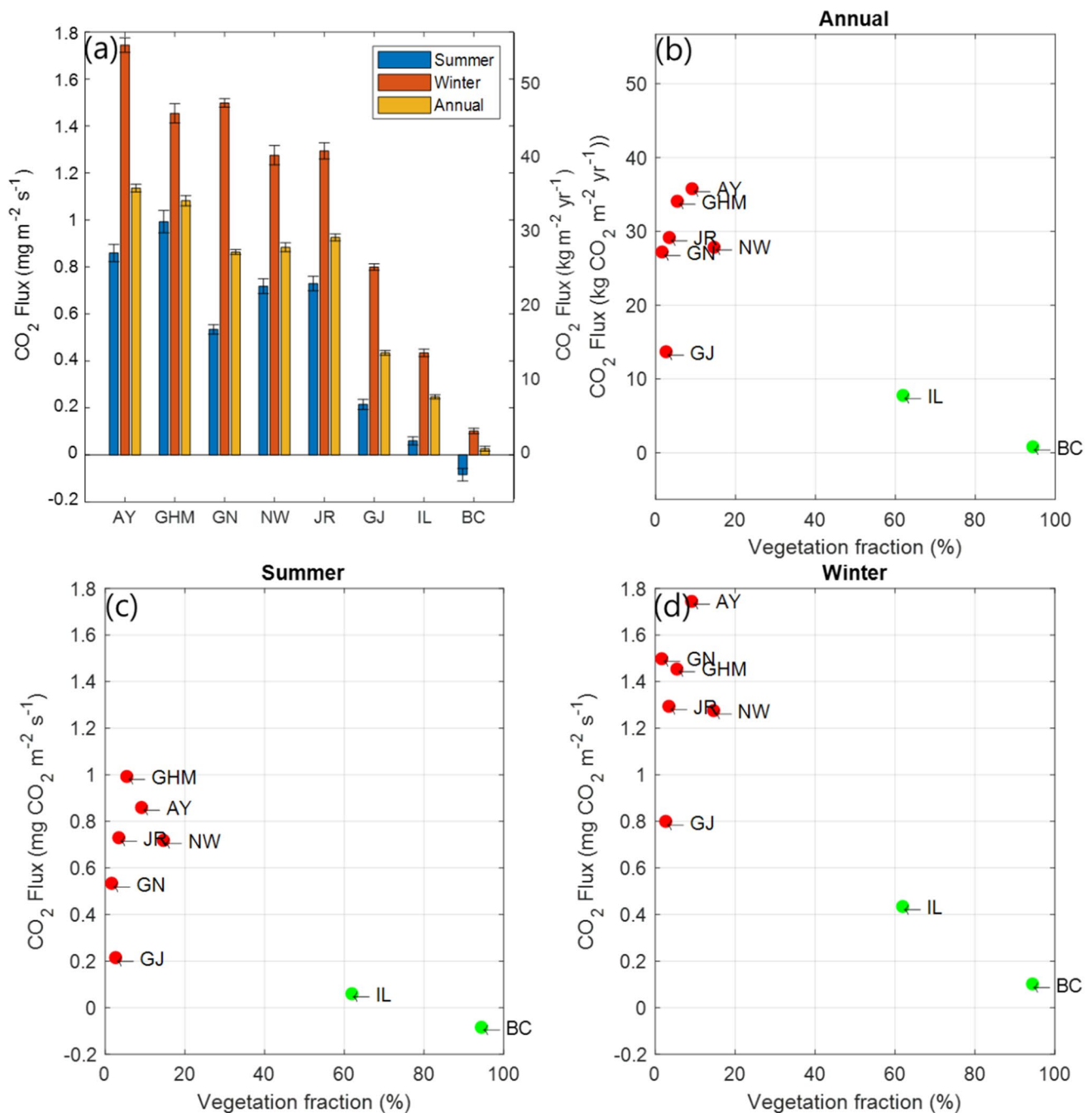


**Fig. 3** (a) The summer (blue), winter (red) and annual (orange) CO<sub>2</sub> fluxes in the 2017–2018 period. The error bars in (a) indicate the 95% confidence interval based on Student's-t tests. Figures 3(b)–(d) show the relationship between the vegetation-area fraction and the

(b) annual, (c) summer, and (d) winter CO<sub>2</sub> fluxes at the eight SEB sites. Red and green dots in Figs. 3b–d indicate the urban and suburban sites, respectively

but are absent in winter (blue lines in Fig. 4) at the two suburban sites. Note that the CO<sub>2</sub> flux diurnal cycle at both suburban sites is much weaker, nearly nonexistent, in winter than in summer. The daytime minima in the annual-mean diurnal cycle (black lines in Fig. 4) at the two suburban sites show that photosynthesis plays a crucial role in determining the CO<sub>2</sub> budget for summer and for the entire year. The

differences in the CO<sub>2</sub> fluxes between the two suburban sites may be attributed to the differences in the vegetation-area fraction (61.9% for IL and 94.4% for BC) and the road fraction (28.4% for IL and 1.9% for BC) (Table 2), i.e., the effects of traffic at IL is much larger than those at BC.

CO<sub>2</sub> fluxes exhibit clear seasonal cycles at all sites with winter maxima and summer minima (Fig. 5a). From late



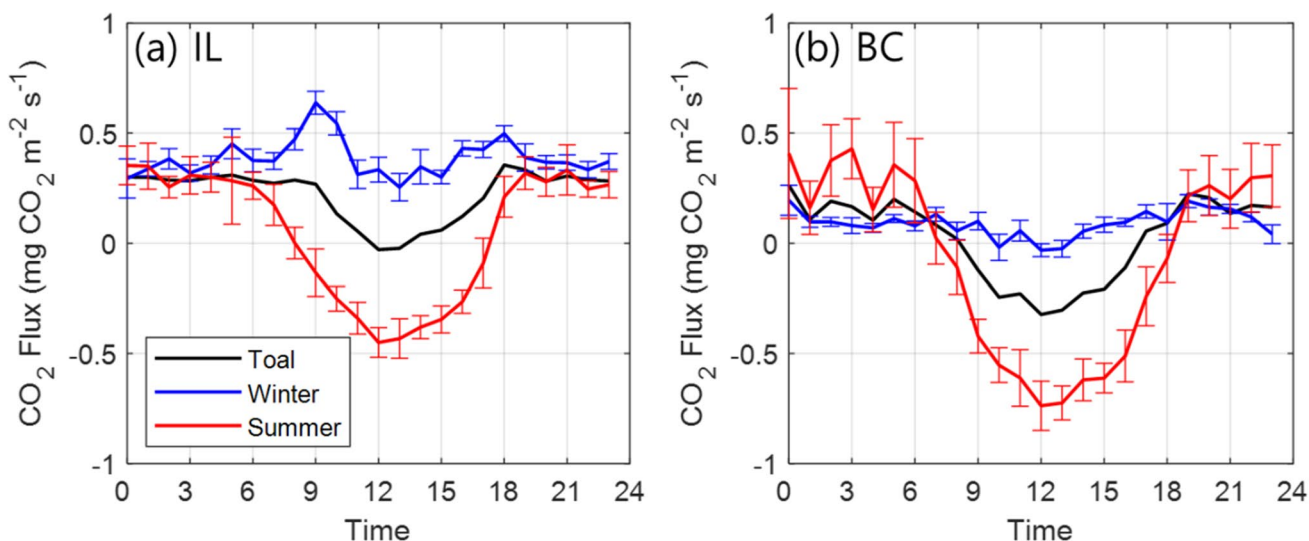


**Fig. 4** The annual (black), summer (red) and winter (blue) CO<sub>2</sub> flux diurnal cycle at the two suburban sites, (a) IL and (b) BC. The error bars indicate the 95% confidence interval based on Student's-t tests

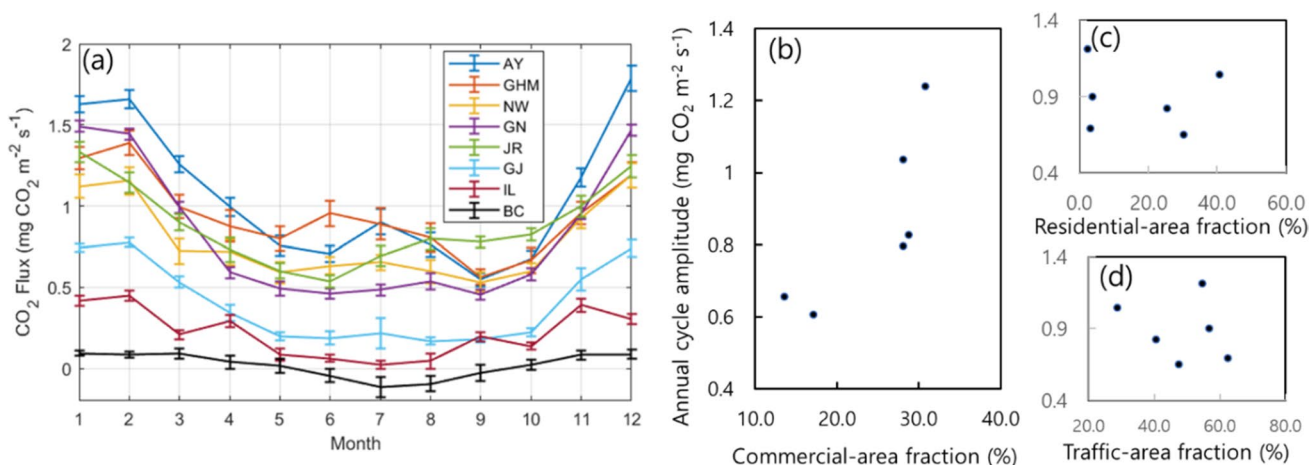


**Fig. 5** (a) The seasonal variations of the CO<sub>2</sub> fluxes at the eight SEB sites. The error bars in (a) indicate the 95% confidence interval based on Student's-t tests. Figure 5(b)-(d) present the relationship between

the amplitude of the CO<sub>2</sub> flux annual cycle and the fraction of the (b) commercial area, (c) residential area, and (d) traffic area at the six urban site

spring to summer, CO<sub>2</sub> fluxes at the two suburban sites are near zero (IL) and -0.2 mg m<sup>-2</sup> s<sup>-1</sup> (BC), demonstrating the critical effects of photosynthesis on the CO<sub>2</sub> flux in the regions of large vegetation cover. The seasonal cycle varies across the sites with the most notable contrast between the urban and suburban sites; the seasonal cycle shows much larger amplitudes at the urban sites (0.7–1.2 mgCO<sub>2</sub> m<sup>-2</sup> s<sup>-1</sup>) than at the suburban sites (0.2–0.5 mgCO<sub>2</sub> m<sup>-2</sup> s<sup>-1</sup>) where anthropogenic emissions sources are small. The positive correlation (R > 0.887) between the monthly CO<sub>2</sub> flux in Fig. 5a and the liquefied natural gas (LNG) consumption (<http://data.seoul.go.kr>) for the six urban sites supports that winter heating is the main driver of the CO<sub>2</sub> flux seasonal variations

at the urban sites (Park et al. 2014, 2022). The seasonal cycle amplitudes at all urban sites are well correlated (R = 0.82) with the commercial-area fraction (Fig. 5b), but are poorly correlated with the traffic- (R = -0.22) and residential-area fraction (R = -0.12) (Figs. 5c,d).

The CO<sub>2</sub> flux at the six urban sites shows distinct relationship with the fractional coverage of land-use types (Table 3). The annual and seasonal CO<sub>2</sub> fluxes are positively correlated with the commercial-area fraction, while they are negatively correlated with the residential-area fraction. The relationship between the CO<sub>2</sub> fluxes and the commercial-area fraction is largest for winter (R = 0.72) followed by for the entire year (R = 0.65) and for summer (0.52). Thus, the CO<sub>2</sub> fluxes at

**Table 3** The correlation between the annual and seasonal CO<sub>2</sub> fluxes at the six urban sites and the fractional area of the major urban land-use types of each site

Land-use fraction	Annual	Summer	Winter
Traffic	0.25	0.43	0.02
Commercial	0.65	0.52	0.72
Residential	-0.60	-0.73	-0.39

the urban sites increase (decrease) with increasing commercial (residential) area fraction, implying that the commercial areas emit more CO<sub>2</sub> per area than the residential areas.

### 3.2 The Relative Contribution of Traffic and Heating to the Seasonal Cycle

Relative contributions of traffic and heating, the two leading CO<sub>2</sub> emissions sources in urban areas, to the total CO<sub>2</sub> fluxes are estimated using the bivariate regression analysis of Kleingeld et al. (2018) where the hourly CO<sub>2</sub> fluxes, traffic volume and ambient temperature are incorporated as in Eqs. (2) and (3). Note that traffic and heating are the primary sources of the observed CO<sub>2</sub> fluxes at these sites because none of them are affected by power plants and/or major manufacturing facilities (e.g., Velasco et al. 2007).

$$F_C = a * (b - T_{air}) + c * veh \text{ if } (b - T_{air}) \leq 0 \quad (2)$$

$$F_C = c * veh \text{ if } (b - T_{air}) \geq 0 \quad (3)$$

$F_C$  (mg m<sup>-2</sup> s<sup>-1</sup>) is the total CO<sub>2</sub> fluxes,  $veh$  (the number of vehicles hr<sup>-1</sup>) is the traffic volume, and  $T_{air}$  (K) is the ambient temperature.  $b$  in Eqs. (2) and (3), the threshold temperature (K) for the start of heating, is also obtained in the regression in the original formulation; however, a threshold temperature of 18°C (291.15 K), the standard temperature for calculating the heating degree days (Lee et al. 2014b), is used in this study for simplicity. A sensitivity test in which  $b$  is varied from 16°C to 19°C, a reasonable range for the start of heating in Seoul, yields the same conclusions as reported in this study except that the relative contribution of heating decreases monotonically with increasing  $b$ . Previous studies (Lee et al. 2014b; Park et al. 2014) showed that ambient temperatures can be a good indicator for the CO<sub>2</sub> emissions from heating in Seoul since large seasonal variations in the ambient temperatures govern the heating demand.

Statistically significant results (the p-values are below 10<sup>-47</sup>) are obtained for three of the four sites at which traffic data are available. Using the regression parameters in Table 4, the fractional contribution of traffic ( $c * veh$ ) and heating ( $a * (b - T_{air})$ ) to the monthly CO<sub>2</sub> flux at the three

**Table 4** Parameters for Eqs. (2) and (3) obtained with the least square method

Site	R <sup>2</sup>	Parameter	Estimate	p-value	t-stat
<b>GHM</b>	0.218	a	0.02325	3.76 × 10 <sup>-47</sup>	14.605
		c	0.00061	0	47.824
<b>GN</b>	0.348	a	0.04777	0	62.455
		c	0.00029	0	51.976
<b>GJ</b>	0.307	a	0.02654	0	46.555
		c	0.00017	2.89 × 10 <sup>-183</sup>	30.378

sites are calculated. The resulting fractional contribution of traffic and heating to the total CO<sub>2</sub> fluxes (Fig. 6) exhibits clear seasonal cycles to show that heating (traffic) is the primary contributor to the observed CO<sub>2</sub> fluxes in the cold (warm) season. As the traffic remains nearly the same over the entire year (Fig. 6d-f), the CO<sub>2</sub> flux seasonal cycle at these sites is related to the seasonal variations in heating. The results also show that the relative contribution from traffic and heating varies following the area fraction of the land-use type in such a way that the contribution of heating increases as the combined fraction of the residential and commercial areas (i.e., the building-area fraction) increases (Table 2), most notably in the cold season. The seasonal variations in the observed CO<sub>2</sub> fluxes (Fig. 5) and the relative contribution of heating to the total CO<sub>2</sub> fluxes (Fig. 6) coincide well with the monthly LNG consumption, the primary heating fuel in Seoul (Lee et al. 2014a). The correlation coefficients between the monthly contribution of heating to the CO<sub>2</sub> fluxes and the monthly LNG consumption at the three sites range from 0.958 to 0.969; the high correlations further support that heating is the main driver of the CO<sub>2</sub> flux seasonal cycle at the urban sites as inferred from the relationship between the amplitude of the CO<sub>2</sub> flux annual cycle and the LNG consumption in the preceding section.

An estimation on the basis of the population density of the Seoul Metropolitan area and the average per-human CO<sub>2</sub> emission (Christen et al. 2011) shows that human respiration may contribute 10–20% to the total CO<sub>2</sub> flux at these sites which is similar to the amounts estimated in previous studies (Christen et al. 2011; Kleingeld et al. 2018; Velasco and Roth 2010). It is not negligible for the total CO<sub>2</sub> budget, however, is not included in the analysis because (1) local population density remains nearly the same for each month and (2) the CO<sub>2</sub> fluxes from human respiration is small compared to those from traffic and heating.

### 3.3 Urban CO<sub>2</sub> Flux Weekly Cycle Related to the Land-Use and Business Types

In order to understand the intra-urban CO<sub>2</sub> flux variations following the land-use and main business types,

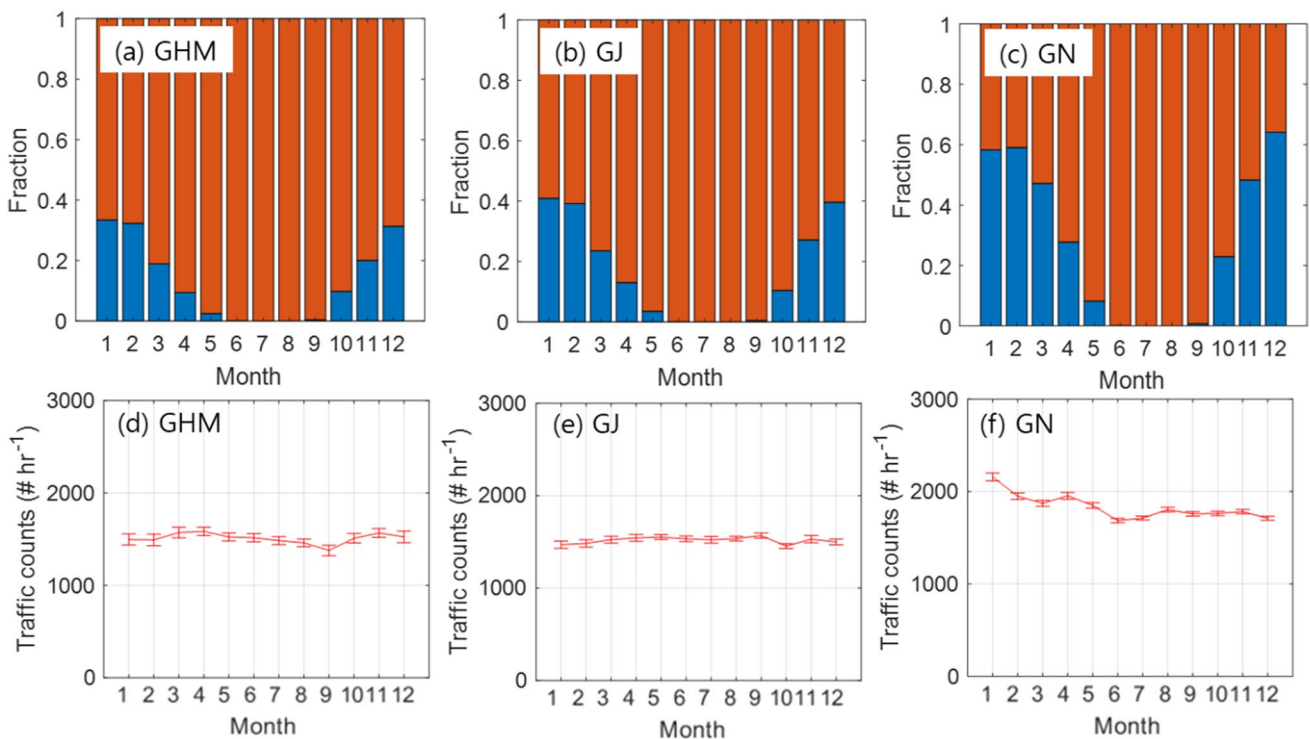


**Fig. 6** The relative contribution of heating (blue) and traffic (red) to the monthly CO<sub>2</sub> fluxes at the three urban sites obtained from the regression analysis in Sect. 3.2: (a) GHM, (b) GJ, and (c) GN. Figures 6d-f present the monthly traffic volume at the three sites

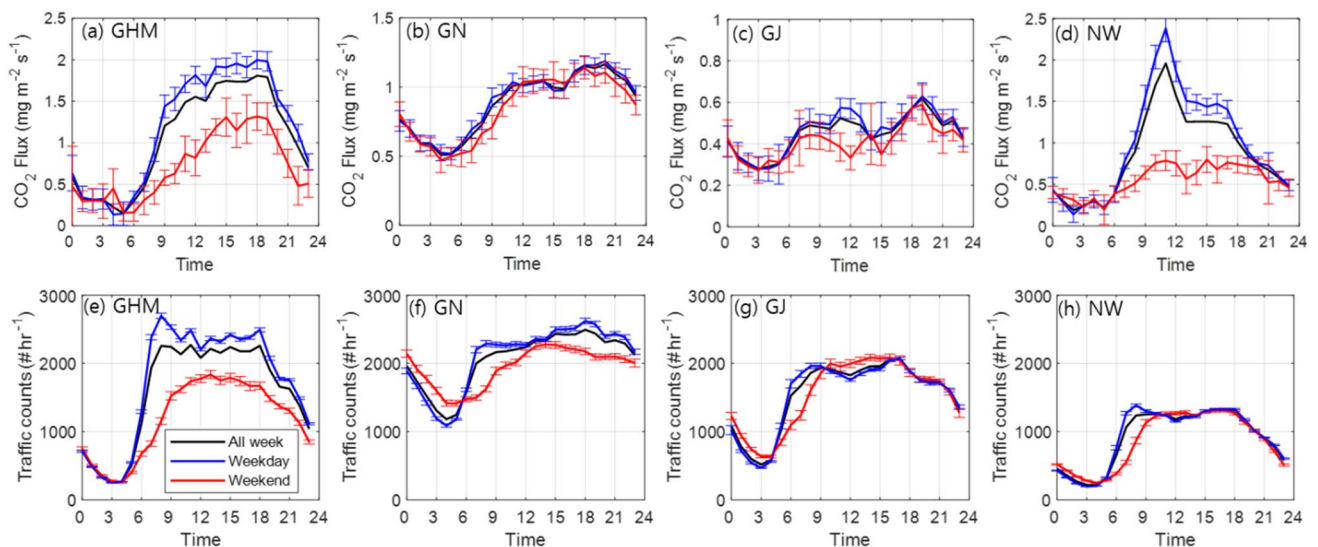


**Fig. 7** The annual-mean CO<sub>2</sub> flux diurnal cycles for the entire week (black), weekdays (blue), and weekends (red with error bars) at the four urban sites; (a) GHM, (b) GN, (c) GJ, and (d) NW. Figures (e)-(h) are the diurnal cycles of the corresponding traffic volume. The error bars indicate the 95% confidence intervals

the weekly cycle of CO<sub>2</sub> fluxes (Fig. 7a-c) and traffic (Fig. 7d-f) are analyzed for the four urban sites (GHM, GN, GJ, NW) where hourly traffic data are available. Because the sub-daily to weekly variations of urban CO<sub>2</sub>

fluxes are closely related to local traffic (Dragomir et al. 2012; Hong et al. 2020; Kleingeld et al. 2018; Velasco et al. 2010), the CO<sub>2</sub> flux variations at these urban sites may reflect specific effects of land-use and business types

(Sect. 2.1) in shaping local traffic. The two sites GHM and GN include similar commercial-area fraction (28.8% at GHM and 28.1% at GN), but show highly contrasting weekly cycles in the CO<sub>2</sub> fluxes and traffic. GHM shows substantially larger CO<sub>2</sub> fluxes and traffic during weekdays than weekends (Figs. 7a,e) while the CO<sub>2</sub> flux and traffic remain similar throughout a week at GN (Figs. 7b,f). The mainly residential GJ shows similar traffic and CO<sub>2</sub> emissions for both weekdays and weekends (Fig. 7c,g). The CO<sub>2</sub> flux-traffic relationship at NW is peculiar; while the traffic is similar for both weekdays and weekends (Fig. 7h), weekdays show much larger CO<sub>2</sub> fluxes than weekends, especially in the daytime hours (Fig. 7d).

The land-use and main business types at each site may explain the weekly cycle of the CO<sub>2</sub> fluxes at the four sites in terms of the CO<sub>2</sub> flux-traffic relationship. GHM and GN include similar commercial-area fractions (28.8% vs. 28.1%) but show highly contrasting business types; government offices, the headquarters of large companies as well as the businesses related to them for GHM and major shopping and entertainment districts for GN. Because the main businesses at GHM are open only in the business hours in weekdays, the traffic and floating populations around GHM are concentrated in the daytime hours of weekdays to result in large differences in CO<sub>2</sub> fluxes (Fig. 7a) and traffic (Fig. 7e) between weekdays and weekends. GN is located in one of the major shopping and entertainment districts in Seoul which draw large traffic and floating population not only in daytimes but also in evenings and early nights throughout a week. Because of these main business types, the traffic (Fig. 7f) and CO<sub>2</sub> fluxes (Fig. 7b) at GN remain similar for the entire week. The large CO<sub>2</sub> fluxes and traffic in the evening and early night hours are mainly due to various entertainment businesses around GN with partial contributions from the commuting traffic. GJ includes much larger residential area than the commercial area (30.3% vs. 17.1%, Table 2). In addition, the businesses around GJ serve mainly local residents. Thus the traffic around GJ is generated mainly from local activities to result in similar traffic (Fig. 7g) and CO<sub>2</sub> fluxes (Fig. 7c) throughout a week except the absence of commuter-related morning peaks in weekends. The peculiar traffic-CO<sub>2</sub> flux relationship at NW (Figs. 7d and h) can be explained by the major business types within its footprint. Although NW includes a large traffic-area fraction (62.4%), much of the traffic area includes a railway depot and a driver's license driving test facility (Fig. 1e and Fig. 2). As the driving test facility opens only for business hours (the work hours on weekdays), the large daytime CO<sub>2</sub> fluxes in weekdays (Fig. 7d) can be attributed to the emissions from driving test vehicles. Despite the large emissions from the driving test vehicles, they are not captured by the local traffic monitoring system to result in similar traffic volumes for both weekdays and weekends. This causes the large mismatch between the CO<sub>2</sub> fluxes and traffic for the work hours of weekdays.

## 4 Conclusions and Discussions

To understand the CO<sub>2</sub> flux variations within a large urban area, the two-year (2017–2018) CO<sub>2</sub> flux data measured at eight EC-based SEB sites, six urban and two suburban, in Seoul are analyzed. The CO<sub>2</sub> fluxes and their variations obtained in the analyses are interpreted in terms of the local factors related to the CO<sub>2</sub> budget such as vegetation coverage, heating, traffic, and land-use types. For the urban sites, the analyses also consider more detailed land-use type such as the area-fractions of commercial, residential, and the traffic areas as well as the primary businesses types in commercial areas.

The annual CO<sub>2</sub> fluxes vary widely across these sites following the vegetation-area fraction and land-use type, from 0.83 kgCO<sub>2</sub> m<sup>-2</sup> yr<sup>-1</sup> at BC to 35.8 kgCO<sub>2</sub> m<sup>-2</sup> yr<sup>-1</sup> at AY. At the two suburban sites of large vegetation-area fraction and small anthropogenic CO<sub>2</sub> emissions sources, vegetation plays a critical role in shaping the annual and seasonal CO<sub>2</sub> fluxes to result in highly contrasting CO<sub>2</sub> flux diurnal cycles between summer and winter highlighted by the presence (summer) and absence (winter) of large downward CO<sub>2</sub> fluxes in the sunlit hours.

For all urban sites, the effects of vegetation on CO<sub>2</sub> fluxes are negligible as indicated by a weak ( $R < 0.43$ ; statistical significant of  $< 60\%$ ) relationship between the CO<sub>2</sub> fluxes and the vegetation-area fraction for all seasons as well as the entire year. The minimal vegetation effects on the CO<sub>2</sub> budget at the urban sites is not only due to small vegetation-area fractions ( $< 14.7\%$ ) but also (and more likely) due to the fact that, per unit area, anthropogenic CO<sub>2</sub> emissions dominate the effects of vegetation (absorption and emission of CO<sub>2</sub>). This finding in this study contrasts a key conclusion of Park et al. (2022) which argues that vegetation effects are critical in determining the CO<sub>2</sub> budget at the entire urban sites. This study suggests that the large correlation between the monthly NDVI and CO<sub>2</sub> fluxes at the urban areas of small vegetation cover found in Park et al. (2022) is only superficial and has little quantitative implications on the CO<sub>2</sub> budget at highly urbanize areas with small vegetation-area fraction.

The positive (negative) correlations between the annual CO<sub>2</sub> fluxes at the urban sites and the commercial (residential) area fraction indicate that the commercial areas emit more CO<sub>2</sub> per unit area than the residential areas. The winter maxima and summer minima in the CO<sub>2</sub> flux annual cycle at both the urban and suburban sites arise from totally different causes; by the seasonal variations in heating (photosynthesis) at the urban (suburban) sites. The importance of heating in driving the seasonal cycle of urban CO<sub>2</sub> fluxes is supported by strong correlations between the monthly LNG consumption and (1) the CO<sub>2</sub> flux cycle at the urban sites

( $R > 0.887$ ; Fig. 5a) and (2) the contribution of heating to the monthly CO<sub>2</sub> flux from a regression-based source attribution analysis ( $R > 0.958$ ; Fig. 6). The regression-based CO<sub>2</sub> flux source attribution analysis also shows that the fraction of CO<sub>2</sub> fluxes emitted by heating increases with increasing residential-area fraction.

The traffic and CO<sub>2</sub> flux at the commercial sites are found to exhibit distinct weekly cycles related to the main business type. This dependence of the CO<sub>2</sub> flux-traffic relationship on the main business type is not explainable in terms of LCZ and/or the single dominant land-use type that have been used in previous studies to classify site characteristics in urban climate research. This, and the variation of CO<sub>2</sub> fluxes following the area fraction of the commercial and residential areas found in this study, show that proper interpretation and understanding of the CO<sub>2</sub> flux variations in large urban areas require considerations of more refined urban land-use type classifications (e.g., the main business types, the area fraction of each land-use type) beyond the contemporary site-type classification based on a single dominant land-use type and/or LCZ.

Accurate estimates of CO<sub>2</sub> fluxes from large urban areas where a multitude of land-use types, human activities, and natural environment coexist, are important for accounting the global CO<sub>2</sub> emissions. In-situ CO<sub>2</sub> flux measurements are important to estimate CO<sub>2</sub> fluxes as they provide the ground-truth data for understanding the relationship between CO<sub>2</sub> emissions and urban characteristics as well as for evaluating the regional CO<sub>2</sub> emissions estimates based on indirect methods. The large CO<sub>2</sub> flux variations following the land-use and business types found in this study for Seoul show that a dense CO<sub>2</sub> flux network is needed to reliably estimate CO<sub>2</sub> emissions in large urban areas as they include heterogeneous landscapes and a variety of land-use and business types. Establishing a dense EC-based flux observation network for monitoring fine-scale CO<sub>2</sub> fluxes is cost prohibitive. Thus, additional studies on urban CO<sub>2</sub> fluxes in terms of refined relationship between CO<sub>2</sub> fluxes and the types of land-use and business are warranted as a preliminary for establishing cost-effective urban CO<sub>2</sub> flux observation networks in large urban regions.

**Acknowledgements** This work funded by the Korea Meteorological Administration Research and Development Program “Developing Technology for High-Resolution Urban Weather Information Services” under Grant (KMA2018-00627) and “Development and Assessment of Climate Change Scenario” (KMA2018-00321).

**Open Access** This article is licensed under a Creative Commons Attribution 4.0 International License, which permits use, sharing, adaptation, distribution and reproduction in any medium or format, as long as you give appropriate credit to the original author(s) and the source, provide a link to the Creative Commons licence, and indicate if changes were made. The images or other third party material in this article are included in the article's Creative Commons licence, unless indicated otherwise in a credit line to the material. If material is not included in

the article's Creative Commons licence and your intended use is not permitted by statutory regulation or exceeds the permitted use, you will need to obtain permission directly from the copyright holder. To view a copy of this licence, visit <http://creativecommons.org/licenses/by/4.0/>.

## References

- An, S.M., Kim, D.H., Hong, S.O., Byon, J.Y.: A Fundamental Study for Urban Canopy Layer Analysis and Application Focusing on Seoul Metropolitan Area Urban Weather Service Domain. *Korea Spat Plan Rev* **105**, 101–120 (2020). <https://doi.org/10.15793/kspr.2020.105.007>
- Asefi-Najafabady, S., Rayner, P.J., Gurney, K.R., McRobert, A., Song, Y., Coltin, K., Huang, J., Elvidge, C., Baugh, K.: A multi-year, global gridded fossil fuel CO<sub>2</sub> emission data product: Evaluation and analysis of results. *J. Geophys. Res. Atmos.* **119**, 10213–10231 (2014). <https://doi.org/10.1002/2013JD021296>
- Baldocchi, D., Falge, E., Gu, L., Olson, R., Hollinger, D., Running, S., Anthoni, P., Bernhofer, Ch., Davis, K., Evans, R., Fuentes, J., Goldstein, A., Katul, G., Law, B., Lee, X., Malhi, Y., Meyers, T., Munger, W., Oechel, W., Paw, K.T.U., Pilegaard, K., Schmid, H.P., Valentini, R., Verma, S., Vesala, T., Wilson, K., Wofsy, S.: FLUXNET: A New Tool to Study the Temporal and Spatial Variability of Ecosystem-Scale Carbon Dioxide, Water Vapor, and Energy Flux Densities. *Bull. Am. Meteorol. Soc.* **82**, 2415–34 (2001). [https://doi.org/10.1175/1520-0477\(2001\)082%3c2415:FANTTS%3e2.3.CO;2](https://doi.org/10.1175/1520-0477(2001)082%3c2415:FANTTS%3e2.3.CO;2)
- Barlow, J.B.: Progress in observing and modelling the urban boundary layer. *Urban Clim.* **10**, 216–240 (2014)
- Canadell, J.G., Raupach, M.R., Houghton, R.A.: Anthropogenic CO<sub>2</sub> emissions in Africa. *Biogeosciences* **6**, 463–468 (2009). <https://doi.org/10.5194/bg-6-463-2009>
- Choi, Y., Kang, S.-L., Hong, J., Grimmond, S., Davis, K.J.: A Next-Generation Weather Information Service Engine (WISE) Customized for Urban and Surrounding Rural Areas. *Bull. Am. Meteorol. Soc.* **94**, ES114–117 (2013)
- Christen, A.: Atmospheric measurement techniques to quantify greenhouse gas emissions from cities. *Urban Clim.* **10**, 241–260 (2014). <https://doi.org/10.1016/j.uclim.2014.04.006>
- Christen, A., Coops, N.C., Crawford, B.R., Kellett, R., Liss, K.N., Olchovskic, I., Tooke, T.R., van der Laana, M., Voogt, J.A.: Validation of modeled carbon-dioxide emissions from an urban neighborhood with direct eddy-covariance measurements. *Atmos. Environ.* **45**, 6057–6069 (2011). <https://doi.org/10.1016/j.atmosenv.2011.07.040>
- Coutts, A.M., Beringer, J., Tapper, N.J.: Characteristics influencing the variability of urban CO<sub>2</sub> fluxes in Melbourne, Australia. *Atmos. Environ.* **41**, 51–62 (2007). <https://doi.org/10.1016/j.atmosenv.2006.08.030>
- Crawford, B., Christen, A.: Spatial source attribution of measured urban eddy covariance CO<sub>2</sub> fluxes. *Theor. Appl. Climatol.* **119**, 733–755 (2015). <https://doi.org/10.1007/s00704-014-1124-0>
- Dragomir, C.M., Klaassen, W., Voiculescu, M., Georgescu, L.P., van der Laan, S.: Estimating Annual CO<sub>2</sub> Flux for Lutjewad Station Using Three Different Gap-Filling Techniques. *Sci. World J.* **2012**, 1–10 (2012). <https://doi.org/10.1100/2012/842893>
- Falge, E., Baldocchi, D., Olson, R., Anthoni, P., Aubinet, M., Bernhofer, C., Burba, G., Ceulemans, R., Clement, R., Dolman, H., Granier, A., Gross, P., Grünwald, T., Hollinger, D., Jensen, N.-O., Katul, G., Keronen, P., Kowalski, A., Lai, C.T., Law, B.E., Meyers, T., Moncrieff, J., Moors, E., Munger, J.W., Pilegaard, K., Rannik, Ü., Rebmann, C., Suyker, A., Tenhunen, J., Tu, K., Verma, S., Vesala, T., Wilson, K., Wofsy, S.: Gap filling strategies for defensible annual sums of net ecosystem



- exchange. *Agric for Meteorol.* **107**, 43–69 (2001). [https://doi.org/10.1016/S0168-1923\(00\)00225-2](https://doi.org/10.1016/S0168-1923(00)00225-2)
- Feigenwinter, C., Vogt, R., Christen, A.: Eddy covariance measurements over urban areas. In: Aubinet M, Vesala T, Papale D. (eds.) *Eddy Covariance A Practical Guide to Measurement and Data Analysis*. Springer, Dordrecht (2012). [https://doi.org/10.1007/978-94-007-2351-1\\_16](https://doi.org/10.1007/978-94-007-2351-1_16)
- Foken, Th., Wichura, B.: Tools for quality assessment of surface-based flux measurements. *Agric. for. Meteorol.* **78**, 83–105 (1996). [https://doi.org/10.1016/0168-1923\(95\)02248-1](https://doi.org/10.1016/0168-1923(95)02248-1)
- Gokhale, S.: Traffic flow pattern and meteorology at two distinct urban junctions with impacts on air quality. *Atmos. Environ.* **45**, 1830–1840 (2011). <https://doi.org/10.1016/j.atmosenv.2011.01.015>
- Grimmond, C.S.B., Christen, A.: Flux measurements in urban ecosystems. *Flux Letter - Newsletter of Fluxnet.* **5**, 1–8 (2012)
- Grimmond, C.S.B., King, T.S., Cropley, F.D., Nowak, D.J., Souch, C.: Local-scale fluxes of carbon dioxide in urban environments: methodological challenges and results from Chicago. *Environ. Pollut.* **116**, S243–S254 (2002). [https://doi.org/10.1016/S0269-7491\(01\)00256-1](https://doi.org/10.1016/S0269-7491(01)00256-1)
- Helfter, C., Famulari, D., Phillips, G.J., Barlow, J.F., Wood, C.R., Grimmond, C.S.B., Nemitz, E.: Controls of carbon dioxide concentrations and fluxes above central London. *Atmos Chem Phys.* **11**, 1913–1928 (2011). <https://doi.org/10.5194/acp-11-1913-2011>
- Helfter, C., Tremper, A.H., Halios, C.H., Kotthaus, S., Björkegren, A., Grimmond, C.S.B., Barlow, J.F., Nemitz, E.: Spatial and temporal variability of urban fluxes of methane, carbon monoxide and carbon dioxide above London. UK. *Atmos Chem Phys.* **16**, 10543–10557 (2016). <https://doi.org/10.5194/acp-16-10543-2016>
- Henne, S., Brunner, D., Oney, B., Leuenberger, M., Eugster, W., Bamberger, I., Meinhardt, F., Steinbacher, M., Emmenegger, L.: Validation of the Swiss methane emission inventory by atmospheric observations and inverse modelling. *Atmos. Chem. Phys.* **16**, 3683–3710 (2016). <https://doi.org/10.5194/acp-16-3683-2016>
- Hong, J.W., Hong, J., Chun, J., Lee, Y.H., Chang, L.S., Lee, J.B., Yi, K., Park, Y.S., Byun, Y.H., Joo, S.: Comparative assessment of net CO<sub>2</sub> exchange across an urbanization gradient in Korea based on eddy covariance measurements. *Carbon. Balance. Manag.* **14**, 13 (2019). <https://doi.org/10.1186/s13021-019-0128-6>
- Hong, J.W., Lee, S.D., Lee, K., Hong, J.: Seasonal variations in the surface energy and CO<sub>2</sub> flux over a high-rise, high-population, residential urban area in the East Asian monsoon region. *Int. J. Climatol.* **40**, 4384–4407 (2020). <https://doi.org/10.1002/joc.6463>
- Kanda, M., Inagaki, A., Miyamoto, T., Gryschka, M., Raasch, S.: A New Aerodynamic Parameterization for Real Urban Surfaces. *Bound-Layer Meteorol.* **148**, 357–377 (2013)
- Kennedy, C., Steinberger, J., Gasson, B., Hansen, Y., Hillman, T., Havránek, M., Pataki, D., Phdungsilp, A., Ramaswami, A., Mendez, G.V.: Greenhouse Gas Emissions from Global Cities. *Environ. Sci. Technol.* **43**, 7297–7302 (2009). <https://doi.org/10.1021/es900213p>
- Kennedy, C., Steinberger, J., Gasson, B., Hansen, Y., Hillman, T., Havránek, M., Pataki, D., Phdungsilp, A., Ramaswami, A., Mendez, G.V.: Methodology for inventorying greenhouse gas emissions from global cities. *Energy Policy* **38**, 4828–4837 (2010). <https://doi.org/10.1016/j.enpol.2009.08.050>
- Kleingeld, E., Hove, B. van, Elbers, J., Jacobs, C.: Carbon dioxide fluxes in the city centre of Arnhem, A middle-sized Dutch city. *Urban Clim.* **17** (2018). <https://doi.org/10.1016/j.uclim.2017.12.003>
- Kljun, N., Calanca, P., Rotach, M.W., Schmid, H.P.: A simple two-dimensional parameterisation for Flux Footprint Prediction (FFP). *Geosci. Model Dev.* **8**, 3695–3713 (2015). <https://doi.org/10.5194/gmd-8-3695-2015>
- Kurppa, M., Nordbo, A., Haapanala, S., Järvi, L.: Effect of seasonal variability and land use on particle number and CO<sub>2</sub> exchange in Helsinki. Finland. *Urban Clim.* **13**, 94–109 (2015). <https://doi.org/10.1016/j.uclim.2015.07.006>
- Labzovskii, L.D., Jeong, S., Parazoo, N.: Working towards confident spaceborne monitoring of carbon emissions from cities using Orbiting Carbon Observatory-2. *Remote Sensing of Environ.* **233**, 111359 (2019)
- Lauvaux, T., Miles, N.L., Deng, A., Richardson, S.J., Cambaliza, M.O., Davis, K.J., Brian Gaudet, B., Gurney, K.R., Huang, J., O’Keefe, D., Song, Y., Karion, A., Oda, T., Patarasuk, R., Razlivanov, I., Sarmiento, D., Shepson, P., Sweeney, C., Turnbull, J., Wu, K.: High-resolution atmospheric inversion of urban CO<sub>2</sub> emissions during the dormant season of the Indianapolis Flux Experiment (INFLUX). *J. Geophys. Res. Atmos.* **121**, 5213–5236 (2016). <https://doi.org/10.1002/2015JD024473>
- Lee, I.H., Ahn, Y.H., Park, J., Kim, S.D.: District Energy Use Patterns and Potential Savings in the Built Environment: Case Study of Two Districts in Seoul. South Korea. *Asian J. Atmos. Environ.* **8**, 48–58 (2014a). <https://doi.org/10.5572/ajae.2014.8.1.048>
- Lee, K., Baek, H.-J., Cho, C.: The Estimation of Base Temperature for Heating and Cooling Degree-Days for South Korea. *J. Appl. Meteorol. Climatol.* **53**, 300–309 (2014b)
- Lee, K., Hong, J.W., Kim, J., Hong, J.: Traces of urban forest in temperature and CO<sub>2</sub> signals in monsoon East Asia. *Atmos Chem Phys* **21**, 17833–17853 (2021)
- Lietzke, B., Vogt, R., Feigenwinter, C., Parlow, E.: On the controlling factors for the variability of carbon dioxide flux in a heterogeneous urban environment. *Int. J. Climatol.* **35**, 3921–3941 (2015). <https://doi.org/10.1002/joc.4255>
- Manning, A.J., O’Doherty, S., Jones, A.R., Simmonds, P.G., Derwent, R.G.: Estimating UK methane and nitrous oxide emissions from 1990 to 2007 using an inversion modeling approach. *J. Geophys. Res.* **116**, D02305 (2011). <https://doi.org/10.1029/2010JD014763>
- Moncrieff, J.B., Massheder, J.M., de Bruin, H., Elbers, J., Friborg, T., Heusinkveld, B., Kabat, P., Scott, S., Soegaard, H., Verhoef, A.: A system to measure surface fluxes of momentum, sensible heat, water vapour and carbon dioxide. *J. Hydrol.* **188–189**, 589–611 (1997). [https://doi.org/10.1016/S0022-1694\(96\)03194-0](https://doi.org/10.1016/S0022-1694(96)03194-0)
- Moncrieff, J.B., Clement, R., Finnigan, J., Meyers, T.: Averaging, detrending and filtering of eddy covariance time series. In: Lee, X., Massman, W.J., Law, B.E. (eds.) *Handbook of micrometeorology: a guide for surface flux measurements*, pp. 7–31. Kluwer Academic, Dordrecht (2004)
- Moriwaki, R., Kanda, M.: Seasonal and Diurnal Fluxes of Radiation, Heat, Water Vapor, and Carbon Dioxide over a Suburban Area. *J Appl Meteorol.* **43**, 1700–1710 (2004). <https://doi.org/10.1175/JAM2153.1>
- Nemitz, E., Hargreaves, K.J., McDonald, A.G., Dorsey, J.R., Fowler, D.: Micrometeorological Measurements of the Urban Heat Budget and CO<sub>2</sub> Emissions on a City Scale. *Environ Sci Technol. American Chemical Society.* **36**, 3139–3146 (2002). <https://doi.org/10.1021/es010277e>
- Park, M.S., Joo, S.J., Park, S.: Carbon dioxide concentration and flux in an urban residential area in Seoul. Korea. *Adv Atmos Sci.* **31**(5), 1101–1112 (2014)
- Park, M.S., Park, S.H., Chae, J.H., Choi, M.H., Song, Y., Kang, M., Roh, J.W.: High-resolution urban observation network for user-specific meteorological information service in the Seoul Metropolitan Area. South Korea. *Atmos. Meas. Tech.* **10**, 1575–1594 (2017). <https://doi.org/10.5194/amt-10-1575-2017>
- Park, C., Jeong, S., Park, H., Yun, J., Liu, J.: Evaluation of the potential use of satellite-derived XCO<sub>2</sub> in detecting CO<sub>2</sub> enhancement in megacities with limited ground observations: A case study in Seoul using Orbiting Carbon Observatory-2. *Asia-Pac. J. Atmos. Sciences* (2020). <https://doi.org/10.1007/s13143-020-00202-5>

- Park, C., Jeong, S., Shin, Y., Cha, Y., Lee, H.: Reduction in urban atmospheric CO<sub>2</sub> enhancement in Seoul, South Korea, resulting from social distancing policies during the COVID-19 pandemic. *Atmos. Pollut. Res.* **12**, 101176 (2021). <https://doi.org/10.1016/j.apr.2021.101176>
- Park, C., Jeong, S., Park, M.S., Park, H., Yun, J., Lee, S.S., Park, S.-H.: Spatiotemporal variations in urban CO<sub>2</sub> flux with land-use types in Seoul. *Carb Balance Management* **17** (2022). <https://doi.org/10.1186/s13021-022-00206-w>
- Pawlak, W., Fortuniak, K., Siedlecki, M.: Carbon dioxide flux in the centre of Łódź, Poland—analysis of a 2-year eddy covariance measurement data set. *Int. J. Climatol.* **31**, 232–243 (2011). <https://doi.org/10.1002/joc.2247>
- Peters, W., Jacobson, A.R., Sweeney, C., Andrews, A.E., Conway, T.J., Masarie, K., Miller, J.B., Bruhwiler, L.M.P., Pétron, G., Hirsch, A.I., Worthy, D.E.J., van der Werf, G.R., Randerson, J.T., Wennberg, P.O., Krol, M.C., Tans, P.P.: An atmospheric perspective on North American carbon dioxide exchange: CarbonTracker. *Proc. Natl. Acad. Sci. USA* **104**, 18925–18930 (2007). <https://doi.org/10.1073/pnas.0708986104>
- Raupach, M.R., Antonia, R.A., Rajagopalan, S.: Rough-wall turbulent boundary layers. *Appl. Mech. Rev.* **44**, 1–25 (1991). <https://doi.org/10.1115/1.3119492>
- Sargent, M., Barrera, Y., Nehrkorn, T., Hutyrá, L.R., Gately, C.K., Jones, T., McKain, K., Sweeney, C., Hegarty, J., Hardiman, B., Wang, J.A., Wofsy, S.C.: Anthropogenic and biogenic CO<sub>2</sub> fluxes in the Boston urban region. *Proc. Natl. Acad. Sci. USA* **115**, 7491–7496 (2018). <https://doi.org/10.1073/pnas.1803715115>
- Satterthwaite, D.: Cities' contribution to global warming: notes on the allocation of greenhouse gas emissions. *Environ. Urban.* **20**(2), 539–549 (2008). <https://doi.org/10.1177/0956247808096127>
- Shim, C., Han, J., Henze, D.K., Yoon, T.: Identifying local anthropogenic CO<sub>2</sub> emissions with satellite retrievals: a case study in South Korea. *Int. J. Remote Sensing* **40**(3), 1011–1029 (2019)
- Soegaard, H., Møller-Jensen, L.: Towards a spatial CO<sub>2</sub> budget of a metropolitan region based on textural image classification and flux measurements. *Remote Sens. Environ.* **87**, 283–294 (2003). [https://doi.org/10.1016/S0034-4257\(03\)00185-8](https://doi.org/10.1016/S0034-4257(03)00185-8)
- Stagakis, S., Chrysoulakis, N., Spyridakis, N., Feigenwinter, C., Vogt, R.: Eddy Covariance measurements and source partitioning of CO<sub>2</sub> emissions in an urban environment: Application for Heraklion, Greece. *Atmos. Environ.* **201**, 278–292 (2019). <https://doi.org/10.1016/j.atmosenv.2019.01.009>
- Stewart, I.D., Oke, T.R.: Local Climate Zones for Urban Temperature Studies. *Bull Am Meteorol Soc.* **93**, 1879–1900 (2012). <https://doi.org/10.1175/BAMS-D-11-00019.1>
- UN, Department of Economic and Social Affairs, Population Division. *World Urbanization Prospects: the 2018 Revision (ST/ESA/SER.A/420)* (2019). <https://population.un.org/wup/Publications/Files/WUP2018-Report.pdf>. Accessed 27 October 2022
- UNFCCC. Decision 1/CP.21. Adoption of the Paris Agreement. (2015). <https://unfccc.int/sites/default/files/resource/docs/2015/cop21/eng/10a01.pdf>. Accessed 27 October 2022
- Velasco, E., Roth, M.: Cities as Net Sources of CO<sub>2</sub>: Review of Atmospheric CO<sub>2</sub> Exchange in Urban Environments Measured by Eddy Covariance Technique: Urban CO<sub>2</sub> flux measurements by eddy covariance. *Geogr. Compass* **4**, 1238–1259 (2010). <https://doi.org/10.1111/j.1749-8198.2010.00384.x>
- Velasco, E., Pressley, S., Allwine, E., Westberg, H., Lamb, B.: Measurements of CO<sub>2</sub> fluxes from the Mexico City urban landscape. *Atmos Environ.* **39**, 7433–7446 (2005). <https://doi.org/10.1016/j.atmosenv.2005.08.038>
- Velasco, E., Lamb, B., Westberg, H., Allwine, E., Sosa, G., Arriaga-Colina, J.L., Jobson, B.T., Alexander, M.L., Prazeller, P., Knighton, W.B., Rogers, T.M., Grutter, M., Herndon, S.C., Kolb, C.E., Zavala, M., de Foy, B., Volkamer, R., Molina, L.T., Molina, M.J.: Distribution, magnitudes, reactivities, ratios and diurnal patterns of volatile organic compounds in the Valley of Mexico during the MCMA 2002–2003 field campaigns. *Atmos Chem Phys.* **7**, 329–353 (2007). <https://doi.org/10.5194/acp-7-329-2007>
- Velasco, E., Roth, M., Tan, S.H., Quark, M., Nabarro, S.D.A., Norford, L.: The role of vegetation in the CO<sub>2</sub> flux from a tropical urban neighborhood. *Atmos. Chem. Phys.* **13**, 10185–10202 (2013). <https://doi.org/10.5194/acp-13-10185-2013>
- Vickers, D., Mahrt, L.: Quality Control and Flux Sampling Problems for Tower and Aircraft Data. *J. Atmos. Ocean. Technol.* **14**, 512–526 (1997). [https://doi.org/10.1175/1520-0426\(1997\)014%3c0512:QCAFSP%3e2.0.CO;2](https://doi.org/10.1175/1520-0426(1997)014%3c0512:QCAFSP%3e2.0.CO;2)
- Vogt, R., Christen, A., Rotach, M.W., Roth, M., Satyanarayana, A.N.V.: Temporal dynamics of CO<sub>2</sub> fluxes and profiles over a Central European city. *Theor. Appl. Climatol.* **84**, 117–126 (2006). <https://doi.org/10.1007/s00704-005-0149-9>
- Ward, H.C., Kotthaus, S., Grimmond, C.S.B., Bjarkeggen, A., Wilkinson, M., Morrison, W.T.J., Evans, J.G., Morrison, J.I.L., Iamarino, M.: Effects of urban density on carbon dioxide exchanges: Observations of dense urban, suburban and woodland areas of southern England. *Environ Pollut.* **198**, 186–200 (2015). <https://doi.org/10.1016/j.envpol.2014.12.031>
- Webb, E.K., Pearman, G.I., Leuning, R.: Correction of flux measurements for density effects due to heat and water vapour transfer. *Q.J.R. Meteorol. Soc.* **106**, 85–100 (1980). <https://doi.org/10.1002/qj.49710644707>
- Weissert, L.F., Salmond, J.A., Schwendenmann, L.: A review of the current progress in quantifying the potential of urban forests to mitigate urban CO<sub>2</sub> emissions. *Urban Clim.* **8**, 100–125 (2014). <https://doi.org/10.1016/j.uclim.2014.01.002>

**Publisher's Note** Springer Nature remains neutral with regard to jurisdictional claims in published maps and institutional affiliations.

